

Epithelial Tissue Growth Dynamics: Universal or Not?

Mahmood Mazarei,^{1,2} Jan Åström,³ Jan Westerholm,⁴ and Mikko Karttunen^{2,5,6}

¹*Department of Mathematics, The University of Western Ontario,
1151 Richmond Street, London, Ontario, Canada N6A 5B7*

²*The Centre for Advanced Materials and Biomaterials Research,
The University of Western Ontario, 1151 Richmond Street, London, Ontario, Canada N6A 3K7*

³*CSC Scientific Computing Ltd, Kägelstranden 14, 02150 Esbo, Finland*

⁴*Faculty of Science and Engineering, Åbo Akademi University, Vattenborgsvägen 3, FI-20500, Åbo, Finland*

⁵*Department of Chemistry, The University of Western Ontario,
1151 Richmond Street, London, Ontario, Canada N6A 5B7*

⁶*Department of Physics and Astronomy, The University of Western Ontario,
1151 Richmond Street, London, Ontario, Canada N6A 3K7*

(Dated: March 31, 2022)

Universality of interfacial roughness in growing epithelial tissue has remained a controversial issue. Kardar-Parisi-Zhang (KPZ) and Molecular Beam Epitaxy (MBE) universality classes have been reported among other behaviors including total lack of universality. Here, we utilize a kinetic division model for deformable cells to investigate cell-colony scaling. With seemingly minor model changes, it can reproduce both KPZ- and MBE-like scaling in configurations that mimic the respective experiments. This result neutralizes the apparent scaling controversy. It can be speculated that this diversity in growth behavior is beneficial for efficient evolution and versatile growth dynamics.

Growth of biological matter, e.g., tumor invasion, depends on complex processes such as the mechanism(s) of proliferation, the physical properties of the microenvironment, and cellular migration that can be dominated either by single cell or collective motion that depend on intercellular interactions and intracellular regulation [1].

Characterization of interfacial growth of cellular colonies is important for understanding the factors that control growth and how they manifest themselves in the kinetics and morphology of cell aggregation. Numerous experimental and computational studies have investigated the effects of biochemical regulation and mechanical factors such as cell-to-cell adhesion and friction, and cell division [2–11]. Typically, growth is characterized by scaling analysis which identifies the underlying mechanisms of growth dynamics by critical exponents.

Self-affinity of the interface width, $w(l, t)$, obeys the Family-Vicsek scaling relation [12, 13]

$$w(l, t) \sim t^\beta F(lt^{-\frac{1}{z}}), \quad (1)$$

where the exponent z describes the scaling relation between the critical time and length scales, and can be obtained from the scaling relation $z = \frac{\alpha}{\beta}$, where the exponent α characterizes the roughness of the interface. The exponent β is obtained through the scaling function $F(u) = F(lt^{-\frac{1}{z}})$ which has the following properties: There is a crossover at $u = l_*$. For $u \ll l_*$ the scaling function increases as a power law, $F(u) = u^\beta$, where β is the growth exponent and characterizes the time-dependent dynamics surface roughening. For $u \gg l_*$ the width saturates, and $F(u)$ becomes a constant [14]. With these three critical exponents, interfacial growth is often classified into different dynamic universality classes.

The KPZ equation was the first nonlinear continuum equation used to study surface growth. It is described by

the stochastic differential equation [15]

$$\partial_t h(x, t) = -\lambda [\partial_x h(x, t)]^2 + \nu \partial_x^2 h(x, t) + \xi(x, t), \quad (2)$$

where the height ($h(x, t)$) depends on position and time, and λ, ν and D are physical constants. The first term on the RHS reflects growth that occurs locally normal to the interface and renders the KPZ equation nonlinear. The second term smooths the interface by surface tension ν , and the last term, $\xi(x, t)$, is Gaussian noise given by $\langle \xi(x, t) \rangle = 0$ and $\langle \xi(s, x) \xi(t, y) \rangle = 2D \delta(s - t) \delta(x - y)$. The KPZ universality class is characterized by the exponents $\alpha^{\text{KPZ}} = \frac{1}{2}$, $\beta^{\text{KPZ}} = \frac{1}{3}$, and $z^{\text{KPZ}} = \frac{3}{2}$ [15].

Mathematically, surface tension and lateral growth determine the asymptotic scaling of the KPZ equation. In some growth processes, however, surface diffusion controls the scaling behavior, and the growth process is described by the MBE model [16, 17]

$$\partial_t h(x, t) = -K \partial_x^4 h(x, t) + F + \xi(x, t), \quad (3)$$

where K is the surface diffusion coefficient, F is the growth rate, and $\xi(x, t)$ is Gaussian white noise as in the KPZ equation. The roughness exponents for the MBE universality class for a one dimensional interface are $\alpha^{\text{MBE}} = \frac{3}{2}$, $\beta^{\text{MBE}} = \frac{3}{8}$, and $z^{\text{MBE}} = 4.0$.

Brú *et al.* studied cellular growth using cells from 15 different *in vitro* cell lines and 16 *in vivo* types of tumor cells obtained from patients [7, 8]. They determined the growth to belong to the MBE universality class in all cases with exponents $\alpha = 1.5 \pm 0.15$, $\beta = 0.38 \pm 0.07$, and $z = 4.0 \pm 0.5$ thus suggesting universal growth dynamics for cells. This conclusion was strongly criticized by Buceta and Galeano [18] who dismissed universality of tumor growth dynamics stating serious flaws in Brú *et al.*'s scaling analysis. In their rebuttal Brú *et al.* [9] restated

their conclusions and wrote "the characteristics of MBE dynamics discussed in Brú *et al.* (2003,1998) have not only been rigorously demonstrated but have served as the basis for a successful antitumor therapy currently under development." A recent study of growth of different brain tumors *in vivo* using fractal and scaling analysis shows similarities with some of the results of Brú *et al.* [19].

In contrast to MBE-like dynamics, Huergo *et al.* [10, 11, 20] reported KPZ scaling for both linearly and radially spreading interfaces of HeLa (cervix cancer) and Vero cell colonies. Galeano *et al.* studied the development of plant cell species *Brassica oleracea* and *B. rapa* under various growing conditions and obtained $\alpha = 0.86 \pm 0.4$, and $z = 5.0$ [21]. Santalla *et al.* [22] grew colonies of *Bacillus subtilis* and *Escherichia coli* using a high agar concentration regime with various nutrients and discovered branching interfaces with exponents $\beta = 0.5$ and $\alpha = 0.75$ that are inconsistent with both MBE and KPZ.

Substrate disorder can also influence growth dynamics. Vicsek *et al.* [23] studied the growth of *E. coli* and *B. subtilis* colonies and found the roughness exponent $\alpha = 0.78 \pm 0.07$ which is inconsistent with both the KPZ and MBE models as well as with the quenched KPZ (qKPZ) model [14] that includes disorder. It has also been demonstrated that the behavior of bacterial colonies in the medium-to-high nutrient concentration regime can be very rich due to the appearance of quenched disorder in growth patterns [24]. In that context, Huergo *et al.* also examined the 2D growth dynamics of quasilinear Vero cell colony fronts in a methylcellulose-containing culture medium. Their scaling analysis yielded $\alpha = 0.63 \pm 0.04$, $\beta = 0.75 \pm 0.05$, and $z = 0.84 \pm 0.05$, suggesting qKPZ dynamics [25].

On the computational and theoretical side, Santalla and Ferreira [26] used an off-lattice Eden model modified to account for nutrient diffusion. Under scarce nutrient supply, they observed initially a KPZ regime that transitioned via a qKPZ transient to unstable growth. Block *et al.* studied the growth of 2D cellular monolayers for a class of cellular automaton models. Their results suggest KPZ dynamics over a wide range of parameters and different cell migration dynamics [27] contradicting the MBE dynamics reported by Brú *et al.* [7]. Another contradiction was reported by Azimzade *et al.* who developed a tumor growth model based on the nonlinear Fisher-Kolmogorov-Petrovsky-Piskunov equation, a reaction-diffusion equation, to investigate the impact of the cellular environment and spatial correlations on tumor invasion [28]. They concluded that kinetic growth models, such as KPZ, cannot characterise tumor invasion fronts, and that the structure of the tumor interface depends intimately on the initial conditions [28].

A large number of different models has been used to describe cellular growth [29]. Here, we use the *CellSim3D* off-lattice growth model and simulator to study epithelial tissue growth [30, 31]. In this model, cells can migrate,

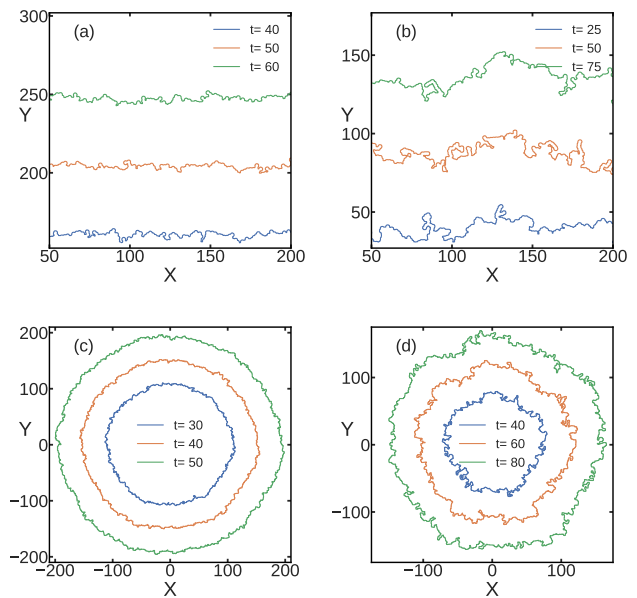


FIG. 1. Interface evolutions of cell colonies starting from a horizontal line and a radially expanding interface. (a) Line configuration at weak (10) and (b) strong cell-cell adhesion (2000). (c) Radially expanding interface with at weak (10) and (d) strong adhesion (2000). All interfaces have overhangs. Scaling analysis was done using overhang-corrected interfaces [14]. For the units, see Table S1.

deform, divide, and interact with each other and their environment mechanically via adhesion and friction. Its 2D version has been shown to produce, e.g., cell-cell force distributions, force dipoles, spontaneous orientation of cells in the direction of highest stiffness and cellular migration in agreement with experiments [32]. *CellSim3D* software leverages graphics processor units, enabling simulations of systems $> 100,000$ cells easily. The analysis below uses averages over 10 independent simulations. Details, parameters and animations demonstrating the model are provided as Supplemental Material. In brief, in *CellSim3D*, epithelial tissues can be modeled as quasi-2D systems of 3D cells confined into a plane, corresponding to the experimental confinement of cells between two plates; the bottom plate models basal tissue and the top plate prevents excessive buckling.

The interface width is defined as the standard deviation of the height over a length scale l at time t as [14]

$$w(l, t) = \left\{ \frac{1}{N} \sum_{i=1}^N [h_i(t) - \langle h_i \rangle_l]^2 \right\}^{\frac{1}{2}}, \quad (4)$$

where L is the contour length, which increases with time as $L = 2\pi \langle h(t) \rangle$ for radially expanding fronts and is constant for linear fronts. For radially expanding fronts, $h_i(t)$ is the distance from the center of mass to the point i of the interface at time t , $\langle h_i \rangle_l$ is the local average of

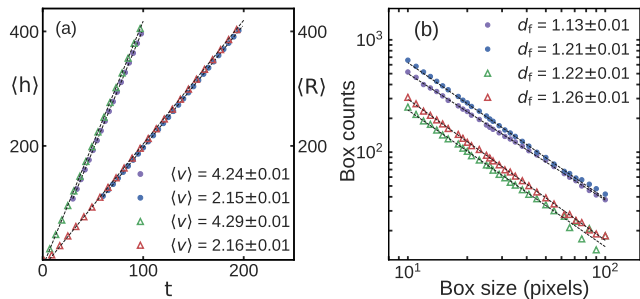


FIG. 2. (a) Velocity ($\langle v \rangle$) of the interface determined from the mean colony radius $\langle R \rangle$ and the mean interface height $\langle h \rangle$ vs. time for different cell-cell adhesion strengths. Radially expanding interface: (purple circles) at weak (10) and (blue circles) strong adhesion (2,000). Line configuration: (green triangles) at weak and (red triangles) at strong adhesion. (b) The fractal dimension (d_f) determined by plotting box counts vs. box size. For radially expanding interface: (purple circles) at weak (10) and (blue circles) strong adhesion (2,000). For line configuration: (green triangles) at weak and (red triangles) strong adhesion. For units, see Table S1.

the subsets of arc length l , and $\{\cdot\}_L$ is the overall average. We complement the universality class analysis by an examination of the structure factor,

$$S(k, t) = \langle \hat{h}(k, t) \hat{h}(-k, t) \rangle, \quad (5)$$

where k is the wavenumber, and $\hat{h}(k, t)$ is the Fourier transform of the interface profile $h(x, t)$ [14]. The advantage of this method over the real space is that only long-wavelength modes contribute to its scaling. Hence, it is less affected by finite-size effects. This method provides the global roughness exponent α and the dynamic exponent z via the Family-Vicsek scaling form for $S(k, t)$,

$$S(k, t) = k^{-2\alpha+1} s(kt^{\frac{1}{z}}), \quad \text{where} \quad (6)$$

$$s(u = kt^{\frac{1}{z}}) = \begin{cases} \text{const} & \text{for } u \gg 1; \\ u^{-2\alpha+1} & \text{for } u \ll 1. \end{cases} \quad (7)$$

At $u = 1$ there is a crossover, for $u \gg 1$ the curves measured at different times collapse and for $u \ll 1$ they split.

We first consider the growth of linear fronts at two different adhesion strengths, 10 (weak) and 2000 (strong), see Table S1 for parameters. The initial configurations had a line of 240 cells, and the final populations consisted of $\approx 200,000$ cells. Snapshots are shown in Fig. 1. As this figure shows, increasing the cell-cell adhesion changes the morphology of the colony and the interface. Figure 2a shows that the interfaces grow at constant velocities with the growth rate decreasing with increasing adhesion.

Next, the box counting method was utilized to determine the fractal dimensions (d_f) of the interfaces for both line configurations (triangles) and radially growing (circles) systems. Figure 2b shows that d_f is in the same

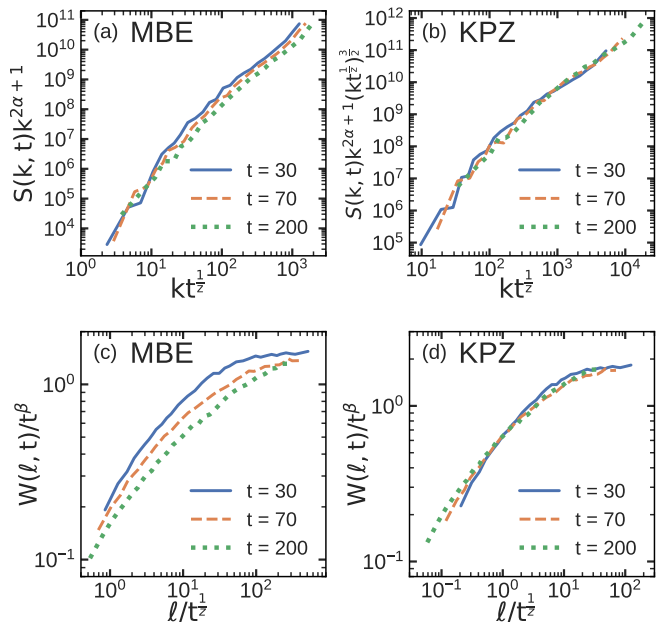


FIG. 3. Data collapse for line growth at high adhesion at three different times. (a) Using the structure factor (Eq. 6) and MBE exponents, $\alpha^{\text{MBE}} = \frac{3}{2}$ and $z^{\text{MBE}} = 4$. (b) With KPZ exponents, $\alpha^{\text{KPZ}} = \frac{1}{2}$ and $z^{\text{KPZ}} = \frac{3}{2}$. The y -axis is scaled with the factor $(kt^{\frac{1}{z}})^{\frac{3}{2}}$ to have the same range as MBE scaling. (c) Using the Family-Vicsek relation for width (Eq. 1) with MBE exponents, $\beta^{\text{MBE}} = \frac{3}{8}$ and $z^{\text{MBE}} = 4$, and (d) with KPZ exponents, $\beta^{\text{KPZ}} = \frac{1}{3}$ and $z^{\text{KPZ}} = \frac{3}{2}$. For units, see Table S1.

range for all simulations. In both geometries, however, d_f is slightly higher for the case of strong adhesion. This is consistent with the experiments of Torres Hoyos *et al.* [19] who reported smaller d_f for malignant and invasive cancer cells as compared to the benign and more solid (higher adhesion) tumors.

Figures 3a-d show the scaling results for line growth both through the width function (Eq. 1) and the structure factor (Eq. 6). As the figure shows, both approaches suggest KPZ dynamics; using the Family-Vicsek relation for the structure factor (Eq. 6) displays slightly better collapse for KPZ than for MBE, Figs. 3a,b, and using width, Eq. 1, the data collapses to a single function using the KPZ exponents (Fig. 3d).

Figure S1 shows that interface roughness, $w(t)$, follows a power-law t^β with $\beta^{\text{weak}} = 0.28 \pm 0.01$ and $\beta^{\text{strong}} = 0.25 \pm 0.02$ for weak and strong adhesion, respectively. Figures S2 and S3 show the local and global roughness exponents. As the figures show, determining the roughness exponent is questionable especially in the case of weak adhesion. The value $\alpha_{\text{loc}}^{\text{strong}} = 0.62 \pm 0.02$, was calculated using width, and $\alpha_{\text{glob}}^{\text{weak}} = 0.75 \pm 0.04$ and $\alpha_{\text{glob}}^{\text{strong}} = 0.52 \pm 0.02$, using the structure factor. As the results show, α_{glob} decreases with increasing adhesion.

Next, we focus on radially expanding isotropic fronts.

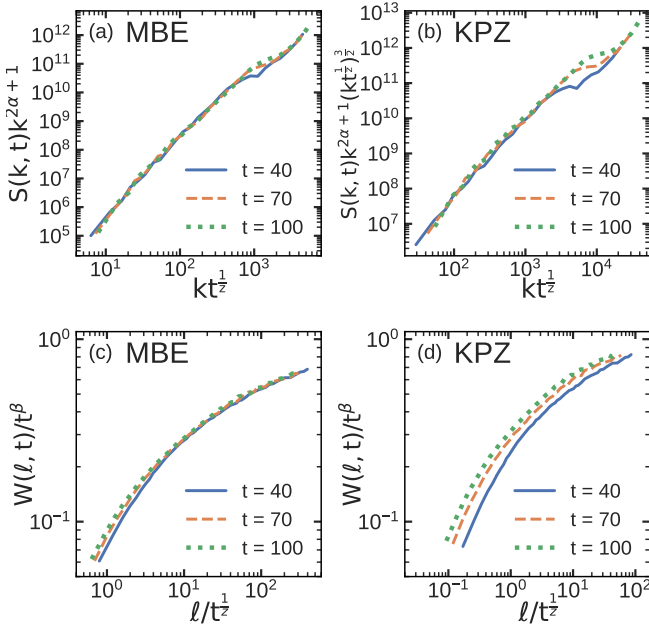


FIG. 4. Data collapse for the radially growing interface at low adhesion at three different times. (a) Using the structure factor (Eq. 6) with MBE, $\alpha^{\text{MBE}} = \frac{3}{2}$ and $z^{\text{MBE}} = 4$ and (b) KPZ exponents, $\alpha^{\text{KPZ}} = \frac{1}{2}$ and $z^{\text{KPZ}} = \frac{3}{2}$. The y -axis is scaled with the factor $(kt^{\frac{1}{z}})^{\frac{3}{2}}$ to have the same range as MBE scaling. (c) Using the Family-Vicsek relation for width (Eq. 1) with MBE exponents, $\beta^{\text{MBE}} = \frac{3}{8}$ and $z^{\text{MBE}} = 4$, and (d) with KPZ exponents, $\beta^{\text{KPZ}} = \frac{1}{3}$ and $z^{\text{KPZ}} = \frac{3}{2}$. For units, see Table S1.

The initial configuration was one cell at the center of the simulation box and the final populations were $\approx 200,000$ cells. We define $R_i(t)$ to be the distance from the center of mass of the colony to the i th site at the interface. Snapshots at different times and adhesion strengths are shown in Fig. 1; increasing the adhesion between the cells changes the colony morphology and increases overhangs. The radii grow at constant velocities, $\langle v \rangle = 4.24 \pm 0.01$ for weak and $\langle v \rangle = 2.15 \pm 0.01$ for strong adhesion, Fig. 2a. As in the linear case, increasing the adhesion causes the front velocities to decrease. Again, the fractal dimension (Fig. 2b) shows slight increase with increasing adhesion, $d_f^{\text{weak}} = 1.13 \pm 0.01$ and $d_f^{\text{strong}} = 1.21 \pm 0.01$.

Figures 4a-d show the scaling results for radial growth both through the width function (Eq. 1) and structure factor (Eq. 6). Using the Family-Vicsek relation for width (Fig. 4c) with MBE exponents displays good collapse. In addition, the structure factors at different times show good collapse with MBE exponents.

Figure S4 shows that fitting the width vs time gives the growth exponents $\beta^{\text{weak}} = 0.40 \pm 0.04$ and $\beta^{\text{strong}} = 0.42 \pm 0.06$. For varying adhesion strengths, the local roughness exponent, α_{loc} , are all within the same range: $\alpha_{\text{loc}}^{\text{weak}} = 0.66 \pm 0.01$ and $\alpha_{\text{loc}}^{\text{strong}} = 0.7 \pm 0.01$, Fig. S5. The scaling exponent α_{glob} , measured from the structure fac-

tor, shows a decrease with increasing adhesion strength, $\alpha_{\text{glob}}^{\text{weak}} = 0.95 \pm 0.04$ and $\alpha_{\text{glob}}^{\text{strong}} = 0.71 \pm 0.02$, Fig. S6.

Finally, to test the generality of the above observations, cell-medium friction, intermembrane friction, cell division rules, and the number of cell types with different stiffness were tested using the radially growing system. Figure S7 shows that α_{glob} is insensitive to changes in factors such as cell-medium friction, intermembrane friction, cell division rules, and the number of cell types with different stiffness. These results suggest that dynamics of the radially growing colonies are well described by MBE-like scaling when at weak cell-cell adhesion.

In conclusion, we have demonstrated that weak cell-cell adhesion and an isotropically growing colony display MBE-like scaling for the boundary roughness. This is consistent with the experiments of Brú *et al.* [7]; we digitized their data and show its scaling in Fig. S8. In contrast, a colony growing from a single line of cells, and with strong cell-cell adhesion displays KPZ-like scaling. This is in agreement with the experiments of Huergo *et al.* [10]. In all the studied cases the fractal dimensions of the interface are within the range 1.13–1.26, which is also consistent with prior experiments [7, 10, 11, 20, 21], regardless of the growth scaling behavior.

All the studied cases show linear growth with constant velocity. This is consistent with experiments: Brú *et al.* reported radially spreading cell colonies to exhibit exponential growth in the early stages followed by linear growth [7]. Huergo *et al.* showed that once the number of cells exceeds 700–1,000, radially spreading colonies grow with a constant velocity [11, 20]. Constant velocity also applies for line growth [10]. Physically, these data suggest that cells are partially contact-inhibited and that most activity occurs within a limited band along the interface challenging the notion of Gompertzian growth of cancer [33]. Experiments by Costa *et al.* indicate that *in vitro* cultivated cells may exhibit sigmoidal growth [3].

Finally, it can be assumed that the first multi-cellular life-forms were rather simple cell colonies. It is interesting to speculate that if cell-colony growth dynamics would be rigidly confined to a single universality class, adaptive evolution would likely be significantly harder in contrast to more versatile growth dynamics. This is consistent with earlier results in the sense that very rich growth behaviour and diverse tissues appear with modest changes, and, e.g., non-trivial dependencies in initial conditions, nutrients, apoptosis, disorder and mechanical forces from various sources cause changes in both quantitative and qualitative behaviors, see, e.g., Refs. [2, 28, 31, 32, 34].

We thank the Natural Sciences and Engineering Research Council of Canada (MK), Canada Research Chairs Programs (MK) and Western University's Science International Engagement Fund (MM) for financial support. The use of the computational resources provided by the Finnish Grid and Cloud Infrastructure FGCI, funded by the Academy of Finland, is gratefully acknowledged.

-
- [1] S. SenGupta, C. A. Parent, and J. E. Bear, The principles of directed cell migration, *Nat. Rev. Mol. Cell Biol.* **22**, 529 (2021).
- [2] T. Lecuit and L. Le Goff, Orchestrating size and shape during morphogenesis, *Nature* **450**, 189 (2007).
- [3] F. Costa, M. Campos, and M. da Silva, The universal growth rate behavior and regime transition in adherent cell colonies, *J. Theor. Biol.* **387**, 181 (2015).
- [4] J. Li, S. K. Schnyder, M. S. Turner, and R. Yamamoto, Role of the cell cycle in collective cell dynamics, *Phys. Rev. X* **11**, 031025 (2021).
- [5] E. Khain and J. Straetmans, Dynamics of an expanding cell monolayer, *J. Stat. Phys.* **184**, 1 (2021).
- [6] M. Radszuweit, M. Block, J. Hengstler, E. Schöll, and D. Drasdo, Comparing the growth kinetics of cell populations in two and three dimensions, *Phys. Rev. E* **79**, 051907 (2009).
- [7] A. Brú, S. Albertos, J. Luis Subiza, J. L. García-Asenjo, and I. Brú, The universal dynamics of tumor growth, *Biophys. J.* **85**, 2948 (2003).
- [8] A. Brú, J. M. Pastor, I. Feraud, I. Brú, S. Melle, and C. Berenguer, Super-rough dynamics on tumor growth, *Phys. Rev. Lett.* **81**, 4008 (1998).
- [9] A. Brú, S. Albertos, J. L. Subiza, J. L. Garcia-Asenjo, and I. Brú, Reply to comments by Buceta and Galeano regarding the article “The Universal Dynamics of Tumor Growth”, *Biophys. J.* **88**, 3737 (2005).
- [10] M. Huergo, M. Pasquale, A. Bolzán, A. Arvia, and P. González, Morphology and dynamic scaling analysis of cell colonies with linear growth fronts, *Phys. Rev. E* **82**, 031903 (2010).
- [11] M. A. C. Huergo, M. A. Pasquale, P. H. González, A. E. Bolzán, and A. J. Arvia, Dynamics and morphology characteristics of cell colonies with radially spreading growth fronts, *Phys. Rev. E* **84**, 021917 (2011).
- [12] F. Family and T. Vicsek, Scaling of the active zone in the Eden process on percolation networks and the ballistic deposition model, *J. Phys. A* **18**, L75 (1985).
- [13] F. Family, Dynamic scaling and phase transitions in interface growth, *Physica A* **168**, 561 (1990).
- [14] A.-L. Barabási and H. E. Stanley, *Fractal Concepts in Surface Growth* (Cambridge University Press, 1995).
- [15] M. Kardar, G. Parisi, and Y.-C. Zhang, Dynamic scaling of growing interfaces, *Phys. Rev. Lett.* **56**, 889 (1986).
- [16] D. A. Kessler, H. Levine, and L. M. Sander, Molecular-beam epitaxial growth and surface diffusion, *Phys. Rev. Lett.* **69**, 100 (1992).
- [17] S. D. Sarma, S. Ghaisas, and J. Kim, Kinetic super-roughening and anomalous dynamic scaling in nonequilibrium growth models, *Phys. Rev. E* **49**, 122 (1994).
- [18] J. Buceta and J. Galeano, Comments on the Article “The Universal Dynamics of Tumor Growth” by A. Brú et al., *Biophys. J.* **88**, 3734 (2005).
- [19] F. T. Hoyos, R. B. Navarro, J. V. Villadiego, and M. Guerrero-Martelo, Geometrical study of astrocytomas through fractals and scaling analysis, *App. Rad. Isotopes* **141**, 250 (2018).
- [20] M. A. C. Huergo, M. A. Pasquale, P. H. González, A. E. Bolzán, and A. J. Arvia, Growth dynamics of cancer cell colonies and their comparison with noncancerous cells, *Phys. Rev. E* **85**, 011918 (2012).
- [21] J. Galeano, J. Buceta, K. Juárez, B. Pumarino, J. De La Torre, and J. Iriondo, Dynamical scaling analysis of plant callus growth, *Europhys. Lett.* **63**, 83 (2003).
- [22] S. N. Santalla, J. Rodríguez-Laguna, J. P. Abad, I. Marín, M. del Mar Espinosa, J. Muñoz-García, L. Vázquez, and R. Cuerno, Nonuniversality of front fluctuations for compact colonies of nonmotile bacteria, *Phys. Rev. E* **98**, 012407 (2018).
- [23] T. Vicsek, M. Cserző, and V. K. Horváth, Self-affine growth of bacterial colonies, *Physica A* **167**, 315 (1990).
- [24] J. A. Bonachela, C. D. Nadell, J. B. Xavier, and S. A. Levin, Universality in bacterial colonies, *J. Stat. Phys.* **144**, 303 (2011).
- [25] M. A. C. Huergo, N. E. Muzzio, M. A. Pasquale, P. P. González, A. E. Bolzán, and A. J. Arvia, Dynamic scaling analysis of two-dimensional cell colony fronts in a gel medium: A biological system approaching a quenched Kardar-Parisi-Zhang universality, *Phys. Rev. E* **90**, 022706 (2014).
- [26] S. N. Santalla and S. C. Ferreira, Eden model with non-local growth rules and kinetic roughening in biological systems, *Phys. Rev. E* **98**, 022405 (2018).
- [27] M. Block, E. Schöll, and D. Drasdo, Classifying the expansion kinetics and critical surface dynamics of growing cell populations, *Phys. Rev. Lett.* **99**, 248101 (2007).
- [28] Y. Azimzade, A. A. Saberi, and M. Sahimi, Effect of heterogeneity and spatial correlations on the structure of a tumor invasion front in cellular environments, *Phys. Rev. E* **100**, 062409 (2019).
- [29] A. Buttenschön and L. Edelstein-Keshet, Bridging from single to collective cell migration: A review of models and links to experiments, *PLoS Comput. Biol.* **16**, e1008411 (2020).
- [30] P. Madhikar, J. Åström, J. Westerholm, and M. Karttunen, CellSim3D: GPU accelerated software for simulations of cellular growth and division in three dimensions, *Comput. Phys. Comm.* **232**, 206 (2018).
- [31] P. Madhikar, J. Åström, J. Westerholm, B. Baumeier, and M. Karttunen, Coarse-grained modeling of cell division in 3d: influence of density, medium viscosity, and inter-membrane friction on cell growth and nearest neighbor distribution, *Soft Mater.* **18**, 150 (2020).
- [32] P. Madhikar, J. Åström, B. Baumeier, and M. Karttunen, Jamming and force distribution in growing epithelial tissue, *Phys. Rev. Res.* **3**, 023129 (2021).
- [33] A. K. Laird, Dynamics of tumor growth, *Br. J. Cancer* **13**, 490 (1964).
- [34] D. T. Tambe, C. Corey Hardin, T. E. Angelini, K. Rajendran, C. Y. Park, X. Serra-Picamal, E. H. Zhou, M. H. Zaman, J. P. Butler, and D. A. Weitz, Collective cell guidance by cooperative intercellular forces, *Nat. Mater.* **10**, 469 (2011).

Supplemental Material:

Epithelial Tissue Growth Dynamics: Universal or Not?

Mahmood Mazarei,^{1,2} Jan Åström,³ Jan Westerholm,⁴ and Mikko Karttunen^{2,5,6}

¹*Department of Mathematics, The University of Western Ontario,
1151 Richmond Street, London, Ontario, Canada N6A 5B7*

²*The Centre for Advanced Materials and Biomaterials Research,
The University of Western Ontario,
1151 Richmond Street, London, Ontario, Canada N6A 3K7*

³*CSC Scientific Computing Ltd, Kägelstranden 14, 02150 Esbo, Finland*

⁴*Faculty of Science and Engineering, Åbo Akademi University,
Vattenborgsvägen 3, FI-20500, Åbo, Finland*

⁵*Department of Chemistry, The University of Western Ontario,
1151 Richmond Street, London, Ontario, Canada N6A 5B7*

⁶*Department of Physics and Astronomy,
The University of Western Ontario,
1151 Richmond Street, London, Ontario, Canada N6A 3K7*

(Dated: March 31, 2022)

THE *CELLSIM3D* MODEL

CellSim3D [1, 2] is a 3D generalization of the 2D model originally introduced by Mkrtchyan, Åström, and Karttunen [3]. In *CellSim3D* cells are defined as a set of interconnected nodes on the surface of a spherical C180 fullerene. The force field consists of bonded and non-bonded forces defined as

$$\mathbf{F} = m\ddot{\mathbf{r}} = \mathbf{F}^{\text{B}} + \mathbf{F}^{\theta} + \mathbf{F}^{\text{P}} + \mathbf{F}^{\text{R}} + \mathbf{F}^{\text{A}} + \mathbf{F}^{\text{F}} + \eta, \quad (1)$$

where \mathbf{F}^{B} is a damped harmonic oscillator force between neighboring nodes, \mathbf{F}^{θ} is the angle force which preserves cell curvature. These two forces are bonded, and the rest are non-bonded. \mathbf{F}^{R} and \mathbf{F}^{A} are the repulsive and attractive force between C180 nodes in different cells, respectively. They are approximated by harmonic potentials with different spring constants and cutoffs. The model has been shown to produce versatile behavior in agreement with experiments [1–4]. We discuss some of the main features below.

Adhesion forces in living cells are generated by adhesive bonds between Cell Adhesion Molecules (CAMs) on the surface of neighbouring cells [5–7]. Each node on the boundary of the simulated cells behaves as an adhesive site, approximating the average CAM behavior [1]. \mathbf{F}^{F} is the friction term decomposed into viscous drag due to the medium approximating the interactions between the cell and the extracellular matrix, and intermembrane friction, which is proportional to the component of the relative velocity tangential to the surface of the cells [1]. Together attractive, repulsive, and friction terms approximate inter-membrane interactions mediated by cell adhesion molecules [8–12]. Finally, \mathbf{F}^{P} is the growth force coming from the osmotic pressure within cells and the cell’s internal pressure [8], and $\eta \equiv \eta(\mathbf{x}, t)$, is Gaussian white noise.

In *CellSim3D*, growth is induced by increasing the internal pressure, as determined by experimental measurements [13]. At each time step, the internal pressure is incremented, resulting in a increase in the pressure force [1, 14]. As a result, the cell volume gradually increases, $V = V_0 + \Delta V$, and once it exceeds the threshold value, V_{div} , the cell can divide into two new symmetric or asymmetric daughter cells depending on the chosen division rule [15]. In this work, we consider that the daughter cells are symmetric [16, 17].

The cell division plane’s position can be either through the cell’s centre of mass or through another randomly chosen point inside the cell. The random point might be different for each

cell, resulting in asymmetric division. The division plane's orientation can also be set using a variety of rules. According to Hertwig's rule, the division plane is perpendicular to the longest axis of an ellipsoidal cell and passes through the centre of mass [18]. Errera's rule asserts that the division plane must contain the shortest path travelling through the centre of mass of a cell [19]. The division plane can also be randomly oriented. In *CellSim3D*, in the case of full 3D tissue, the division plane vector is chosen randomly from a unit sphere. In the case of 2D epithelial tissue, the division plane is sampled from a unit circle in the epithelial plane [2]. The parameters used in the simulations are listed in Table S1. These parameters are based on the properties of HeLa cells for parameter mapping. For further details and their derivation about the *CellSim3D* force field, methodology, parameter mapping, and code implementation, please see Refs. [1, 3, 20].

ANALYSIS METHODS

The interface local width function, $w(l, t)$, is defined as the standard deviation of the front height, $h(x, t)$, over a length scale l at time t as [21]

$$w(l, t) = \left\{ \frac{1}{N} \sum_{i=1}^N [h_i(t) - \langle h_i \rangle_l]^2 \right\}_L^{\frac{1}{2}}, \quad (2)$$

For small length scales the width function behaves as follows

$$w(l, t) \sim l^{\alpha_{\text{loc}}} \quad (3)$$

where α_{loc} is the local roughness exponent. By replacing l with the system size L , the value of $w(L, t)$ for $t \ll t_s$, where t_s is the roughness saturation time, is expected to increase as

$$w(L, t) \sim t^\beta \quad (4)$$

where β is the growth exponent [21]. We supplement the universality class analysis by an examination of the structure factor, $S(k, t)$, of the interface,

$$S(k, t) = \langle \hat{h}(k, t) \hat{h}(-k, t) \rangle, \quad (5)$$

The linear interface roughness, $w(t)$, follows the power-law t^β with $\beta^{\text{weak}} = 0.28 \pm 0.01$, for weak adhesion and $\beta^{\text{strong}} = 0.25 \pm 0.02$, for strong adhesion, Fig. S1. The local roughness exponents, α_{loc} , are within the same range for different adhesion strengths in the case of

linear interface: $\alpha_{\text{loc}}^{\text{weak}} = 0.59 \pm 0.01$ for weak adhesion and $\alpha_{\text{loc}}^{\text{strong}} = 0.62 \pm 0.02$ for strong adhesion, Fig. S2, The global roughness exponent, α_{glob} , of the linear growing interface was calculated via structure factor analysis, $\alpha_{\text{glob}}^{\text{weak}} = 0.75 \pm 0.04$ and $\alpha_{\text{glob}}^{\text{strong}} = 0.52 \pm 0.02$, Fig. S3. The width functions of the circular interface versus time t^β are displayed in Fig. S4: $\beta^{\text{weak}} = 0.40 \pm 0.04$ for weak adhesion and $\beta^{\text{strong}} = 0.42 \pm 0.06$ for strong adhesion. The local roughness exponents, α_{loc} , for circular interface are $\alpha_{\text{loc}}^{\text{weak}} = 0.66 \pm 0.01$ for weak adhesion and $\alpha_{\text{loc}}^{\text{strong}} = 0.7 \pm 0.01$ for strong adhesion, Fig. S5. Finally, For circular interfaces, we find $\alpha_{\text{glob}}^{\text{weak}} = 0.95 \pm 0.04$ and $\alpha_{\text{glob}}^{\text{strong}} = 0.71 \pm 0.02$, Fig. S6.

ANALYSES ON BRÚ'S DATA SET

Data from Fig. 3 of Brú *et al.* [22] was digitized with the WebPlotDigitizer program [23]. Figure S8 shows the result from using the Family-Vicsek relation to scale the width function by MBE (Fig. S8a) and KPZ (Fig. S8b) exponents. MBE exponents show a better collapse than KPZ exponents, as Brú *et al.* stated in their study. However, we cannot obtain a full collapse for the width functions at different times with MBE exponents, implying that the development dynamics of cell-colony interfaces do not perfectly fit into the MBE universality class. The similar conclusion can be made about Huergo *et al.* results [24–26]. Although they concluded that their data reveal a KPZ growth dynamics for cell-colony growth, their works do not exhibit a full width function or structure factor collapse [24–26].

TABLES

TABLE S1. Each cell’s mechanical properties are determined by the values indicated here. They are usually subtly altered to represent different types of cells. The mechanical properties of cells addressed in this work are listed in the table. The symbol † indicates units of Δt and * units of mean time to cell division, which varies between cell types and is set to 1.0 in *CellSim3D*. For more details and their derivation, please see [1, 3]

| Parameter | Notation | Sim. Units | SI Units | |
|---------------------------|-----------------------|----------------------|----------------------|-----------------------------------|
| Nodes per cell | N_c | 180 | - | |
| Node mass | m | 0.04 | 40 | fg |
| Bond stiffness | k^B | 1000 | 100 | $\frac{\text{nN}}{\mu\text{m}}$ |
| Bond damping coefficient | γ_{int} | 100 | 0.01 | $\frac{\text{g}}{\text{s}}$ |
| Minimum pressure | $(PS)_0$ | 50 | 0.5 | $\frac{\text{nN}}{\mu\text{m}^2}$ |
| Maximum pressure | $(PS)_\infty$ | 65 | 0.65 | $\frac{\text{nN}}{\mu\text{m}^2}$ |
| Pressure growth rate | $\Delta(PS)$ | 0.002 | 2.0×10^{-5} | $\frac{\text{nN}}{\mu\text{m}^2}$ |
| Attraction stiffness | K^A | 10-2000 | 1-200 | $\frac{\text{nN}}{\mu\text{m}}$ |
| Attraction range | R_0^A | 0.3 | 3 | μm |
| Repulsion stiffness | K^R | 10×10^5 | 10×10^4 | $\frac{\text{nN}}{\text{m}}$ |
| Repulsion range | R_0^R | 0.2 | 2 | μm |
| Growth count interval | - | 1000 | † | |
| Inter-membrane friction | γ_{ext} | 1 | 10 | $\frac{\mu\text{g}}{\text{s}}$ |
| Medium friction | γ_{m} | 0.4 | 4 | $\frac{\mu\text{g}}{\text{s}}$ |
| Time step | Δt | 1.0×10^{-4} | * | |
| Threshold division volume | V^{div} | 2.9 | 2900 | μm^3 |

FIGURES

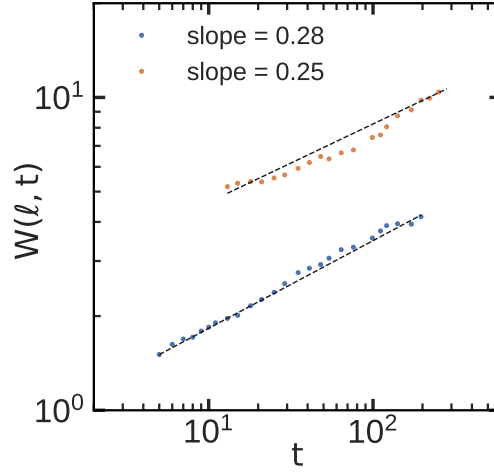


FIG. S1. Log-log plot of the colony interface width vs growth time of the linear interface for different adhesion strength, 10 (blue) and 2,000 (orange). Growth exponents are $\beta^{\text{weak}} = 0.28 \pm 0.01$ and $\beta^{\text{strong}} = 0.25 \pm 0.02$, respectively. For units, see Table S1.

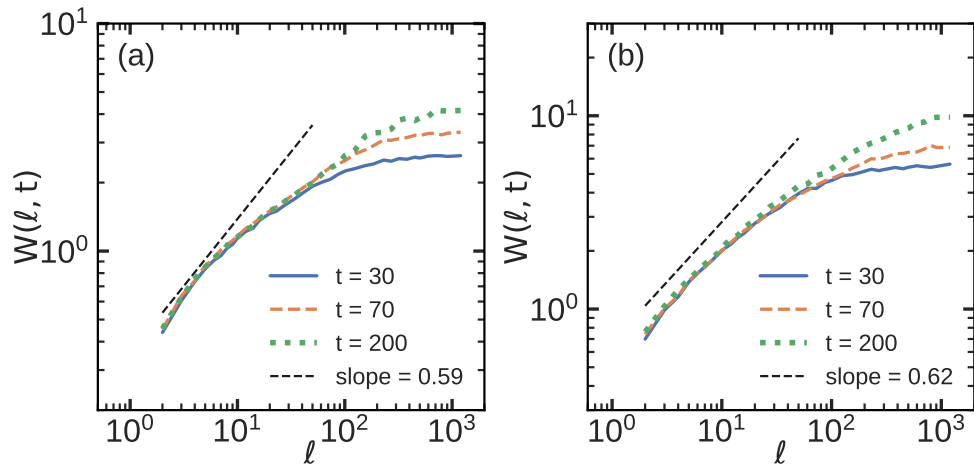


FIG. S2. Log-log plot of the colony interface width of the linear interface vs length l at three different times. (a) weak adhesion strength (10) with $\alpha_{\text{loc}}^{\text{weak}} = 0.59 \pm 0.01$ (b) strong adhesion strength (2,000) with $\alpha_{\text{loc}}^{\text{strong}} = 0.62 \pm 0.02$. For units, see Table S1.

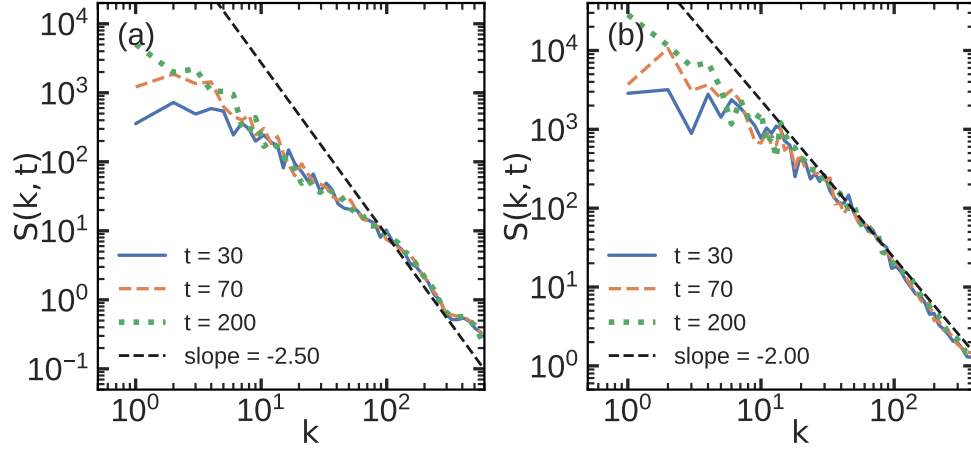


FIG. S3. Log-Log plot of the structure factor at three different times for linear expanding interface. (a) weak adhesion strength (10) with $\alpha_{\text{glob}}^{\text{weak}} = 0.75 \pm 0.04$. (b) strong adhesion strength (2,000) with $\alpha_{\text{glob}}^{\text{strong}} = 0.52 \pm 0.02$. For units, see Table S1.

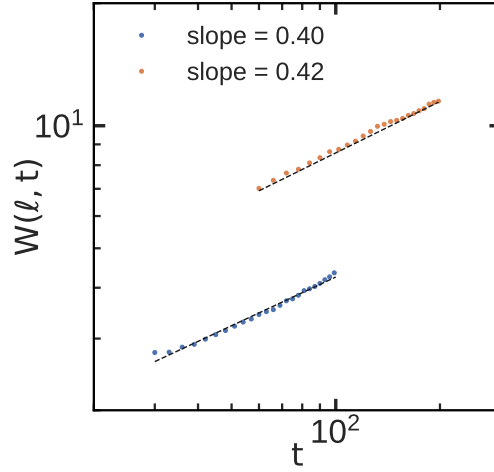


FIG. S4. Log-log plot of the colony interface width vs growth time of the radially expanding interface for different adhesion strength, 10 (Blue) and 2,000 (Orange). Growth exponents are $\beta^{\text{weak}} = 0.40 \pm 0.04$ and $\beta^{\text{strong}} = 0.42 \pm 0.06$, respectively.

-
- [1] P. Madhikar, J. Åström, J. Westerholm, and M. Karttunen, CellSim3D: GPU accelerated software for simulations of cellular growth and division in three dimensions, *Comput. Phys. Comm.* **232**, 206 (2018).

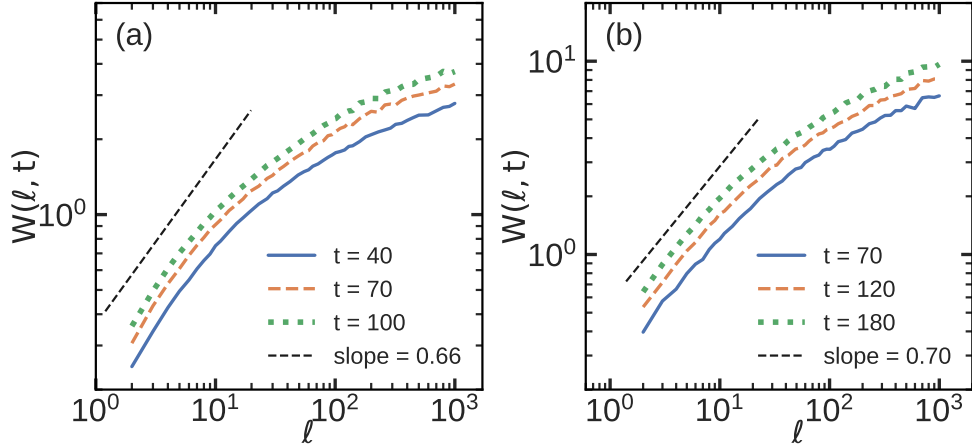


FIG. S5. Log-log plot of the colony interface width of the radially expanding interface vs length ℓ at different times. (a) Weak adhesion strength (10) with slope $\alpha_{\text{loc}}^{\text{weak}} = 0.66 \pm 0.01$, and (b) strong adhesion strength (2,000) with slope $\alpha_{\text{loc}}^{\text{strong}} = 0.70 \pm 0.01$. For units, see Table S1.

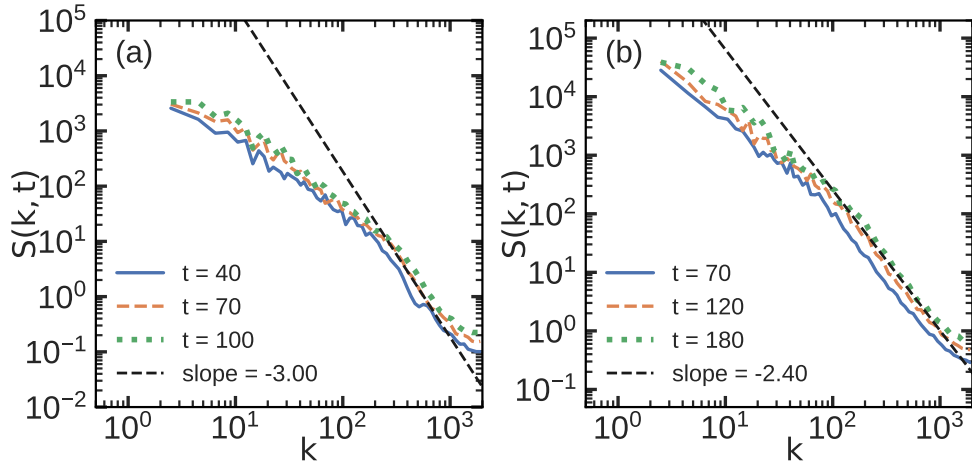


FIG. S6. Log-Log plot of the structure factor at three different times for the radially expanding interface. (a) weak adhesion strength (10) with $\alpha_{\text{glob}}^{\text{weak}} = 0.95 \pm 0.04$, and (b) strong adhesion strength (2000) with $\alpha_{\text{glob}}^{\text{strong}} = 0.71 \pm 0.02$.

- [2] P. Madhikar, J. Åström, J. Westerholm, B. Baumeier, and M. Karttunen, Coarse-grained modeling of cell division in 3d: influence of density, medium viscosity, and inter-membrane friction on cell growth and nearest neighbor distribution, *Soft Mater.* **18**, 150 (2020).
- [3] A. Mkrtychyan, J. Åström, and M. Karttunen, A New Model for Cell Division and Migration with Spontaneous Topology Changes, *Soft Mat.* **10**, 4332 (2014).

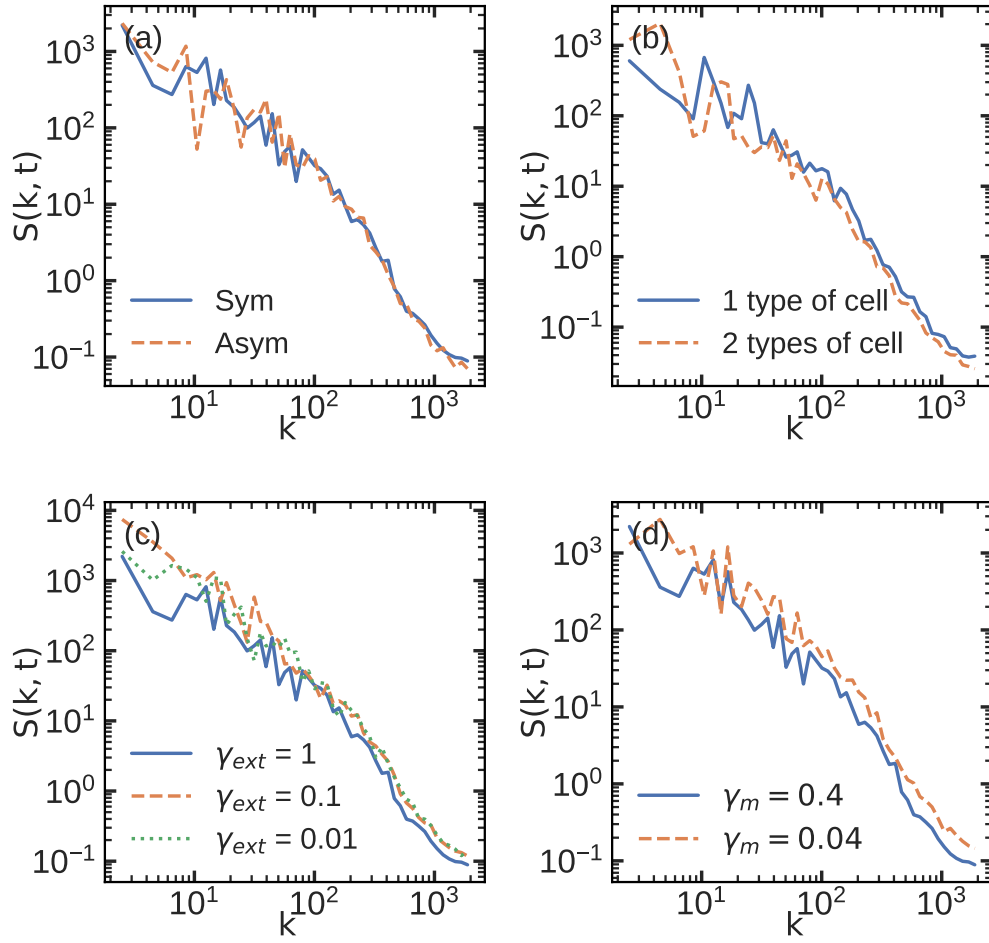


FIG. S7. Log-Log plot of the structure factor of radially expanding interfaces for (a) The division plane is sampled from a unit circle in the epithelial plane, and can yield two symmetric or asymmetric daughter cells in size. (b) The cell population can contain only one type of cell or two types of cells with different stiffness interacting with each others. (c) different friction coefficients for cell-cell interaction, and (d) different medium friction forces. For units, see Table S1.

- [4] P. Madhikar, J. Åström, B. Baumeier, and M. Karttunen, Jamming and force distribution in growing epithelial tissue, *Phys. Rev. Res.* **3**, 023129 (2021).
- [5] F. van Roy and G. Berx, The cell-cell adhesion molecule E-cadherin., *Cell. Mol. Life Sci.* **65**, 3756 (2008).
- [6] M. P. Stemmler, Cadherins in development and cancer., *Mol. Biosyst.* **4**, 835 (2008).
- [7] C. D. Buckley, G. E. Rainger, P. F. Bradfield, G. B. Nash, and D. L. Simmons, Cell adhesion: More than just glue (Review), *Mol. Membr. Biol.* **15**, 167 (1998).

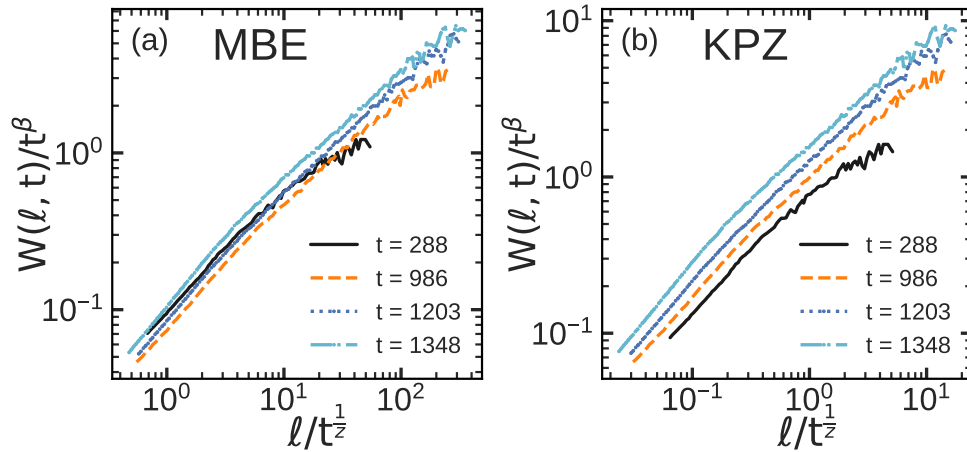


FIG. S8. (a) Data collapse using Family-Vicsek relation for width functions digitized from Fig. 3 from Brú *et al.* [22], at different times with (a) MBE exponents, $\beta = \frac{3}{8}$ and $z = 4$, and (b) KPZ exponents, $\beta = \frac{1}{3}$ and $z = \frac{3}{2}$.

- [8] P. Murray, G. Frampton, and P. Nelson, Cell adhesion molecules, *BMJ* **319**, 332 (1999).
- [9] G. M. Edelman, Cell adhesion molecules, *Science* **219**, 450 (1983).
- [10] G. M. Edelman and K. L. Crossin, Cell Adhesion Molecules: Implications for a Molecular Histology, *Annu. Rev. Biochem.* **60**, 155 (1991).
- [11] D. K. Schluter, I. Ramis-Conde, and M. A. J. Chaplain, Multi-scale modelling of the dynamics of cell colonies: insights into cell-adhesion forces and cancer invasion from in silico simulations, *J. Royal Soc. Interf.* **12**, 20141080 (2014).
- [12] S. van Helvert, C. Storm, and P. Friedl, Mechanoreciprocity in cell migration, *Nat. Cell Biol.* **20**, 8 (2017).
- [13] M. P. Stewart, J. Helenius, Y. Toyoda, S. P. Ramanathan, D. J. Muller, and A. A. Hyman, Hydrostatic pressure and the actomyosin cortex drive mitotic cell rounding, *Nature* **469**, 226 (2011).
- [14] A. Mkrtchyan, *A Single Cell Based Model for Cell Divisions with Spontaneous Topology Changes*, Ph.D. thesis, University of Western Ontario (2013).
- [15] S. J. Morrison and J. Kimble, Asymmetric and symmetric stem-cell divisions in development and cancer, *nature* **441**, 1068 (2006).
- [16] J. Kimble and S. L. Crittenden, Germline proliferation and its control, *WormBook: The Online Review of C. elegans Biology [Internet]* (2005).

- [17] Y. Imoto, Y. Yoshida, F. Yagisawa, H. Kuroiwa, and T. Kuroiwa, The cell cycle, including the mitotic cycle and organelle division cycles, as revealed by cytological observations, *Journal of electron microscopy* **60**, S117 (2011).
- [18] F. Bosveld, O. Markova, B. Guirao, C. Martin, Z. Wang, A. Pierre, M. Balakireva, I. Gaugue, A. Ainslie, N. Christophorou, D. K. Lubensky, N. Minc, and Y. Bellaïche, Epithelial tricellular junctions act as interphase cell shape sensors to orient mitosis, *Nature* **530**, 495 (2016).
- [19] P. Sahlin and H. Jönsson, A Modeling Study on How Cell Division Affects Properties of Epithelial Tissues Under Isotropic Growth, *PLOS ONE* **5**, e11750 (2010).
- [20] P. Jorgensen and M. Tyers, How Cells Coordinate Growth and Division, *Current Biology* **14**, R1014 (2004).
- [21] A.-L. Barabási and H. E. Stanley, *Fractal Concepts in Surface Growth* (Cambridge University Press, 1995).
- [22] A. Brú, S. Albertos, J. Luis Subiza, J. L. García-Asenjo, and I. Brú, The universal dynamics of tumor growth, *Biophys. J.* **85**, 2948 (2003).
- [23] A. Rohatgi, Webplotdigitizer: Version 4.5 (2021).
- [24] M. Huergo, M. Pasquale, A. Bolzán, A. Arvia, and P. González, Morphology and dynamic scaling analysis of cell colonies with linear growth fronts, *Phys. Rev. E* **82**, 031903 (2010).
- [25] M. A. C. Huergo, M. A. Pasquale, P. H. González, A. E. Bolzán, and A. J. Arvia, Dynamics and morphology characteristics of cell colonies with radially spreading growth fronts, *Phys. Rev. E* **84**, 021917 (2011).
- [26] M. A. C. Huergo, M. A. Pasquale, P. H. González, A. E. Bolzán, and A. J. Arvia, Growth dynamics of cancer cell colonies and their comparison with noncancerous cells, *Phys. Rev. E* **85**, 011918 (2012).